Hyperfine Interactions 123/124 (1999) 405–426

Hyperfine spectroscopy in diffraction geometry

R. Rüffer [a], H.D. Rüter [b] and E. Gerdau [b]

[a] *European Synchrotron Radiation Facility, F-38043 Grenoble, France*
[b] *II. Institut für Experimentalphysik, Universität Hamburg, D-22761 Hamburg, Germany*

With the advent of third generation synchrotron radiation sources nuclear Bragg diffraction became a powerful technique for the determination of hyperfine parameters and the electronic and magnetic structure of single crystals. Basic features are discussed theoretically and experimentally and are illustrated by examples such as YIG, $FeBO_3$, α-Fe_2O_3, and Fe_3BO_6.

1. Introduction

Soon after the discovery of the Mössbauer effect first experiments have been reported on nuclear resonant scattering utilizing single crystals. These early investigations dealt mainly with the new phenomenon of pure nuclear reflections and related phenomena such as suppression of the inelastic channel, enhancement and angular dependence of nuclear scattering, anomalous transmission, interference between electronic and nuclear scattering. For a review see the articles of Smirnov and van Bürck [1]. Only a few of these experiments were aimed at the determination of hyperfine parameters. From the experimental point of view diffraction studies with radioactive sources are demanding. Due to the mismatch of the tiny angular acceptance of single crystals (10–50 μrad) and the isotropic emission of radioactive sources the counting rate is very low (0.01–1 Hz) and the requirements on mechanical resolution and stability of the experimental set-up over weeks reached their limits. These facts have prevented a dissemination of this technique.

Replacing the radioactive source by a synchrotron radiation source should overcome these problems. In fact, the small beam size ($\sim$1 mm^2) and divergence ($\sim$20 μrad) favour the use of single crystals. Even though the first successful synchrotron radiation experiments [2–4] have not been performed to determine hyperfine interaction parameters but to study and optimize the demands of a nuclear diffraction set-up at a beam line, it has been shown how easily and precisely these parameters could be derived [5].

In the following we will discuss the advantages of synchrotron radiation for hyperfine spectroscopy in the investigation of single crystals. Especially, we will emphasize the features that are not easily accessible in conventional Mössbauer spectroscopy. In the second part we will give examples for the cases of YIG, $FeBO_3$, Fe_2O_3, and Fe_3BO_6.

2. Nuclear diffraction

The outstanding properties of synchrotron radiation as described in section II.1 of this issue allow one to perform time differential experiments and obtain information on hyperfine parameters as well as on the electric and magnetic structure of the material.

Time differential spectroscopy is not equivalent to the conventional energy differential absorption spectroscopy (Mössbauer spectroscopy (MS)) which averages over the time of formation of the excited state in the source. Time differential experiments are equivalent (by the Fourier transform) to energy differential forward scattering experiments. Therefore, time differential experiments yield more information than the conventional MS. This principal difference manifests itself impressively in the amplitude of the observable effect. In conventional MS it is typically 0.5–10%, whereas in diffraction one observes intensity changes of a factor 3–10.

In a typical Mössbauer experiment one determines besides the isomer shift the magnetic fields and electric field gradients. In this context the asymmetry parameter η is an important quantity, which is, contrary to time differential spectroscopy, not observable in the case of conventional MS with ^{57}Fe. Apart from their amplitudes, for a complete description the orientation of all fields should be determined. For this purpose one needs single crystals. However, the drawback in conventional MS is the need for large single crystals, yet thin enough to allow experiments in transmission geometry. This limits the application of conventional MS to a few examples. Synchrotron radiation, with its small beamsize ($\sim$1 mm^2 unfocussed and $\sim$0.01 mm^2 focussed [6]) allows one to investigate tiny crystals in transmission and in diffraction geometry. For thick crystals diffraction geometry will be preferable. In these cases one might avoid the difficult preparation of a single crystal and the beam can be focussed onto a perfect crystal which is part of a polycrystalline environment.

Another main feature of a diffraction geometry is the easy access to information on the magnetic and electric structure of the crystal. As is known, e.g., from neutron diffraction in the case of antiferromagnetic samples, the crystallographic crystal structure may be superimposed by an electric or/and magnetic structure. These additional structures generate new Bragg reflections which are easily detectable. As in conventional crystallography those structures can be determined from the set of observable reflections. In addition, each observation of a special reflection pattern yields the interaction parameters independently.

Polarized sources were hardly available in the past 40 years for routine experiments in conventional MS. Polarization is a built-in feature of synchrotron radiation, which allows one to select a specific transition for the excitation or to carry out a polarization analysis of the diffracted beam. In any case, taking advantage of polarization very often simplifies the spectra and thus the data evaluation. An impressive example are high pressure experiments with magnetic materials in external magnetic fields (see section IV.2.3 of this issue).

In the case of more complicated structures it is often desirable and possible to excite only subsets of Mössbauer nuclei and to get the information on those parameters

independently. The method allows "site selective" spectroscopy. Having in mind that the synchrotron radiation is in principle white radiation, one has easy access to various Mössbauer transition energies (see section IV.2.7 of this issue) and might extend the site selectivity to sites with different Mössbauer nuclei.

3. Theoretical aspects

The theoretical background of nuclear Bragg diffraction (NBD) has been developed by Hannon and Trammell [7–9] and by Kagan, Afanas'ev and Kohn [10–12] (see also sections III-1.1 and III-1.2 of this issue). As in the case of Coulomb scattering in single crystals, the diffraction process is described by the dynamical theory of X-ray diffraction [13]. However, the Coulomb scattering has to be replaced by the sum of the Coulomb and nuclear scattering amplitude. Due to the strong energy dependence of the nuclear scattering amplitude, i.e., its resonance behaviour, additional new features such as quantum beats, dynamical beats, and speed-up govern the nuclear diffraction process in comparison to pure Coulomb scattering.

The *quantum beat* structure is the main feature in hyperfine spectroscopy for the determination of the nuclear interaction. Furthermore, the strong angular dependence needs careful examination. For the example of $FeBO_3$ given below, this dependence is used to determine the small electric interaction including the sign of V_{zz}. The data evaluation must be carried out in the framework of the dynamical theory. The full formalism is implemented in the program package CONUSS [14] for the Bragg, Laue, and forward diffracted channel. All examples given in this section have been calculated with this package.

For the basic understanding of some features of the spectra it is, however, often useful to consider them in the Born approximation. This has been shown in [15,16], where some extensions have been added in order also to include the speed-up. For nuclear forward scattering (NFS) of the six resonances in α-iron we may also use eqs. (6.24) and (6.26) from section II.2 of this issue. For diffraction, however, one has to introduce the proper spatial phase factors which cause characteristic modifications. In the following we use the notation $\Omega_{\mathrm{M}}(n,m) = \omega_n - \omega_m$, where $\hbar\omega_i$ is the transition energy of line i.

The simplest spectrum is obtained when $\mathbf{k}_{\mathrm{in}} \perp \mathbf{B}_{\mathrm{hf}}$ and $\mathbf{B}_{\mathrm{hf}} \perp \hat{\varepsilon}_{\mathrm{in}} \perp \mathbf{k}_{\mathrm{in}}$. In this case only lines two and five, which are linearly polarized, corresponding to $\Delta m = 0$, are excited and one gets

$$I(t) \propto \mathrm{e}^{-\Gamma t/\hbar}\left[1 + \cos\left(\Omega_{\mathrm{M}}(2,5)\cdot t\right)\right]. \tag{3.1}$$

The beating occurs with a single frequency $\Omega_{\mathrm{M}}(2,5)$ and *maximum contrast*, since both oscillators have equal strength. The factor $\exp(-\Gamma t/\hbar)$ gives the overall damping.

For $\mathbf{k}_{\mathrm{in}} \perp \mathbf{B}_{\mathrm{hf}}$ and $\mathbf{B}_{\mathrm{hf}} \parallel \hat{\varepsilon}_{\mathrm{in}}$ only the $\Delta m = \pm 1$ transitions, which are linearly polarized, will be excited, i.e., lines one, three, four, and six. However, the oscillator strengths are no longer equal but have the ratios 3 : 1 : 1 : 3. One gets a more

complicated beat pattern, which is dominated by the beat frequency of the strong outermost lines, one and six:

$$I(t) \propto \mathrm{e}^{-\Gamma t/\hbar}\left|\cos\left(\frac{1}{2}\Omega_{\mathrm{M}}(1,6)\cdot t\right)+\frac{1}{2}\cos\left(\frac{1}{2}\Omega_{\mathrm{M}}(3,4)\cdot t\right)\right|^2. \tag{3.2}$$

The interference term $\cos((1/2)\Omega_{\mathrm{M}}(1,6)\cdot t)\cos((1/2)\Omega_{\mathrm{M}}(3,4)\cdot t)$ gives rise to a *high–low modulation* of the beating.

Finally, we have the case where $\mathbf{k}_{\mathrm{in}} \parallel \mathbf{B}_{\mathrm{hf}}$ and $\mathbf{B}_{\mathrm{hf}} \perp \hat{\varepsilon}_{\mathrm{in}}$. Again the four transitions with $\Delta m = \pm 1$ are excited, however, now lines one and four are left-circularly polarized while lines three and six are right-circularly polarized. Only transitions of the same polarization state interfere:

$$I(t) \propto \mathrm{e}^{-\Gamma t/\hbar}\left\{\left[1+\frac{3}{5}\cos\big(\Omega_{\mathrm{M}}(1,4)\cdot t\big)\right]+\left[1+\frac{3}{5}\cos\big(\Omega_{\mathrm{M}}(3,6)\cdot t\big)\right]\right\}. \tag{3.3}$$

For $\Omega_{\mathrm{M}}(1,4) = \Omega_{\mathrm{M}}(3,6)$, as, e.g., in α-iron, we get a single beat frequency as in the first case. However, as the strengths of the oscillators involved have the ratios $3:1:1:3$ the beat pattern shows *less contrast*.

In nuclear diffraction spatial phase factors may modify the patterns. For electronically allowed reflections the spatial phase factor does not change the behaviour of the quantum beats. Pure nuclear reflections are electronically forbidden reflections and therefore their scattering amplitudes are out of phase. This changes the cosine function to a sine function, yielding zero intensity at $t = 0$. This is a general feature: pure nuclear reflections always start with zero intensity, whereas "allowed" reflections always start with maximum intensity.

4. Instrumentation

Nuclear diffraction experiments can easily be performed at the new 3rd generation synchrotron radiation sources such as ESRF [17], APS [18], and SPring-8 [19]. However, also 2nd generation sources such as DORIS at HASYLAB [20] are suitable. Normally, the synchrotron beam is delivered by an insertion device of a low emittance machine, providing a small beam size and divergence. The beam is monochromatized in two steps by means of Coulomb scattering in silicon single crystals. The first monochromator that must deal with the high heat-load produced by the synchrotron radiation beam provides an energy bandwidth of some eV. The second, so called high-resolution monochromator, achieves an energy bandwidth of some meV (see section VI.1 of this issue). Typical counting rates are 10^9–10^{10} phot s^{-1} in this bandwidth at 3rd generation synchrotron sources.

The standard sample environment consists of a six circle diffractometer if polarization analysis is included. In the case of the nuclear resonance beamline at the ESRF this diffractometer is applicable to a vertical as well as to a horizontal scattering geometry and this set-up then comprises eight circles. The angular resolutions of the main

circles are typically 1 μrad. For investigations of temperature dependence cryostats or furnaces can be fitted into the diffractometer. Details for the various beamlines may be found on their WEB pages [21].

As detectors avalanche photodiodes (APD) are best suited (see section VI.2 of this issue). The data are recorded either via single channel analysers and fast counters for time integral measurements or/and via a standard set-up for time resolved measurements (time-to-amplitude converter, analog-to-digital converter and multichannel analyzer).

Resonant counting rates in Bragg geometry of 20 kHz in the entire energy band have been reported for α-Fe_2O_3 [22] and of 5 kHz in Γ_0 for $FeBO_3$ [17].

5. Combined hyperfine interaction: garnets

5.1. Structure and symmetry axes

Garnets [23] are excellent candidates to demonstrate the advantages of synchrotron radiation investigations, due to their rich structure. The garnet structure O_h^{10} with site formula $c_3a_2d_3h_{12}$ consists of four crystallographic sites with altogether 160 atoms. Three sites, a, c, and d, may host Mössbauer nuclei, the remaining h-site is occupied by oxygen ions. As an example we will discuss the yttrium iron garnet (YIG).

Big single crystals can be easily grown by the Czrochalski method. However, the samples enriched to about 88% in ^{57}Fe that were used in the following investigations were grown as single crystalline films on gadolinium gallium garnet (GGG) substrates by liquid phase epitaxy. This technique allows one to minimize the amount of ^{57}Fe needed for the production process. Typical crystalline films had diameters of 30 mm and thicknesses between some μm and 50 μm. Their colour is black.

The 40 iron atoms are distributed over 16 a-sites (each surrounded by a distorted oxygen octahedron) and 24 d-sites (each surrounded by a distorted oxygen tetrahedron). The 16 a-sites are further sub-divided into four equal sets by the orientation of the electric field gradient (efg) symmetry axis relative to the cubic crystal axes parallel to the [1 1 1], [$\bar{1}$ 1 1], [1 $\bar{1}$ 1], and [1 1 $\bar{1}$] directions, respectively. The 24 d-sites are further sub-divided into three equal sets by the orientation of the efg symmetry axis with the d_1, d_2, and d_3 sites having their symmetry axes parallel to the [1 0 0], [0 1 0], and [0 0 1] directions, respectively.

In addition to the fixed efg at each site, each iron nucleus is also acted on by an internal hyperfine field $\mathbf{B}_{hf}$. The direction of $\mathbf{B}_{hf}$ may be controlled by an external field $\mathbf{B}_{ext}$. At magnetic saturation, which is already achieved in weak applied fields (see subsection 5.4), $\mathbf{B}_{hf}$ is parallel to the applied field at all a-sites and anti-parallel at the d-sites. At each site the nuclear energy levels are split under the combined influence of $\mathbf{B}_{hf}$ and the efg, with the shift depending on the orientation angle β of $\mathbf{B}_{hf}$ relative to the direction of the efg symmetry axis at that site. More details are given in [24].

5.2. Pure nuclear reflections

Due to the rich structure there exists a large number of pure nuclear reflections, as has been discussed by Winkler et al. [24]. These are the reflections obeying the following rules for the Miller indices hkl with $n, n' \in \mathbb{Z}$:

$$\begin{aligned} &\text{d-sites:} \quad h = 4n + 2, \quad k = l = 4n', \\ &\text{a-sites:} \quad \text{either } h = 2n + 1, \quad k = 2n' + 1, \quad l = 0 \quad \text{or} \\ &\qquad\qquad\qquad h = k = 2n + 1, \quad l = 4n'. \end{aligned}$$

Obviously, pure nuclear reflections exist either for the a-sites or for the d-sites, i.e., both sites never contribute to the same pure nuclear reflection. Vice versa, recording all these reflections simultaneously as is the usual technique in crystallography, e.g., by the Laue method, one could determine the electronic and magnetic structure of the crystal in the same way as one determines the crystallographic structure. The other approach, namely, to measure the time spectra of some selected reflections, may be less time consuming and easier to perform. It yields the same information on the electronic and magnetic structure. As we will see, these spectra depend sensitively not only on the hyperfine parameters, which are the same for each site, but also on the chosen reflection itself. With this method one avoids the difficult corrections on extinction effects and the comparison between intensities of different reflections.

5.3. Site selectivity

As discussed above, the diffraction geometry exhibits a site selectivity. This feature allows one in the case of YIG to investigate independently the a- [25] and d-sites [26]. On the contrary in conventional Mössbauer spectroscopy, also using single crystals, the minimum number of sub-spectra is three, one from one site and two from the other site [24], leading to overlapping sub-spectra, which may cause problems in the data evaluation. In diffraction experiments we may get fewer sub-spectra, as shown in figure 1 for the a-sites and in figure 2 for the d-sites.

These spectra independently reveal the hyperfine parameters of the a-sites and the d-sites. If the c-site would also be occupied by a Mössbauer nucleus as in thulium iron garnet [28] all three sites could be investigated independently. Looking more closely at the diffraction process one sees that for any chosen reflection only two of the a- and d-sites build up the Bragg reflection, while the other a- and d-sites give only rise to absorption. Because the resonances of the a- and d-sites are well separated from each other the absorption by some of the sites influences the diffraction from the other sites only weakly. For this reason the influence of the other sites on the hyperfine parameters is insignificant. However, this also means that the isomer shift of the a-site relative to the d-site can be determined with only low accuracy. It may be determined by NFS where all sites contribute to the spectrum as in conventional Mössbauer spectroscopy.

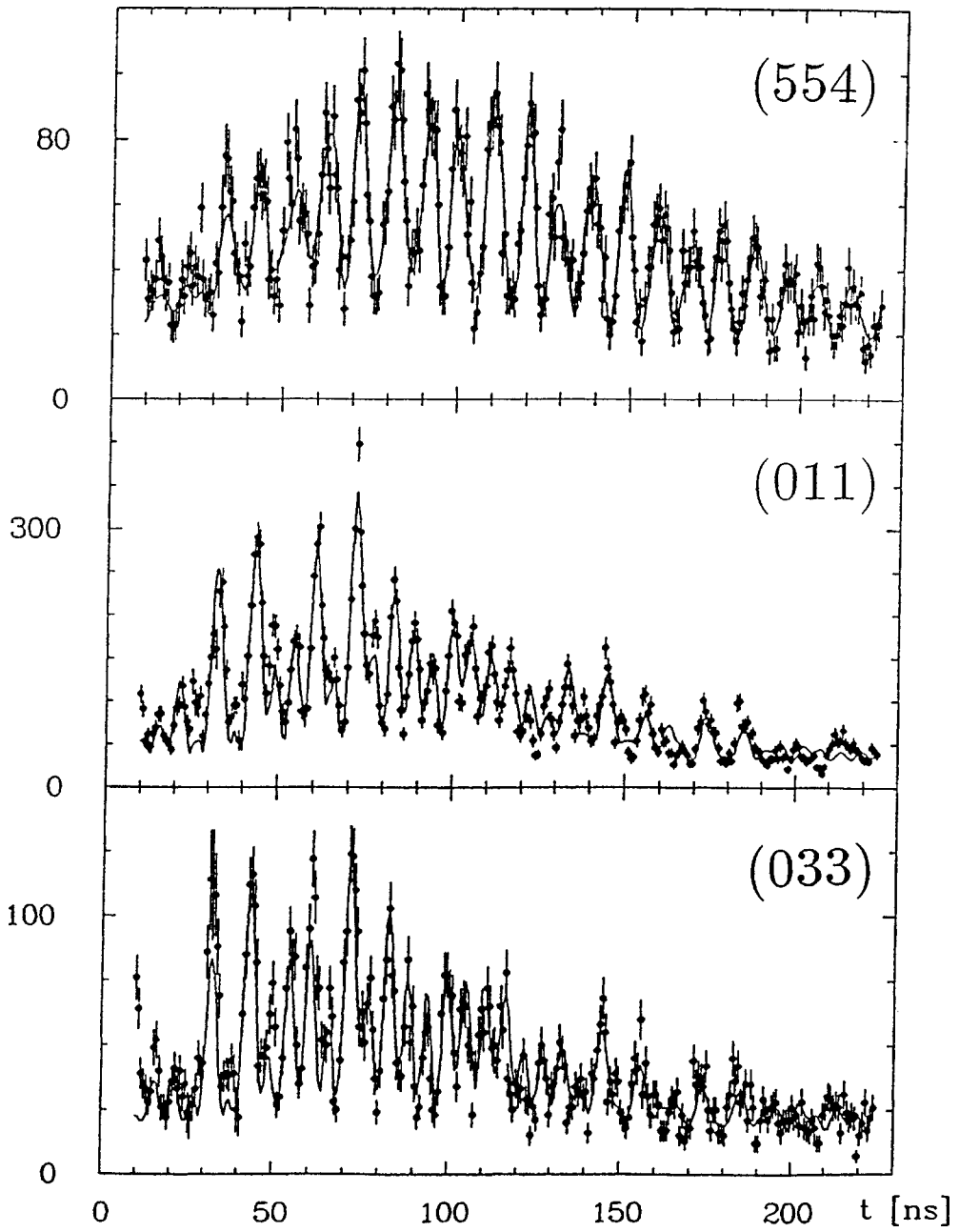

Figure 1. Time spectra of the a-sites in YIG for the (5 5 4), (0 1 1), and (0 3 3) pure nuclear reflections. In all cases only the a_1- and a_2-sites contribute to the reflection (from [25]).

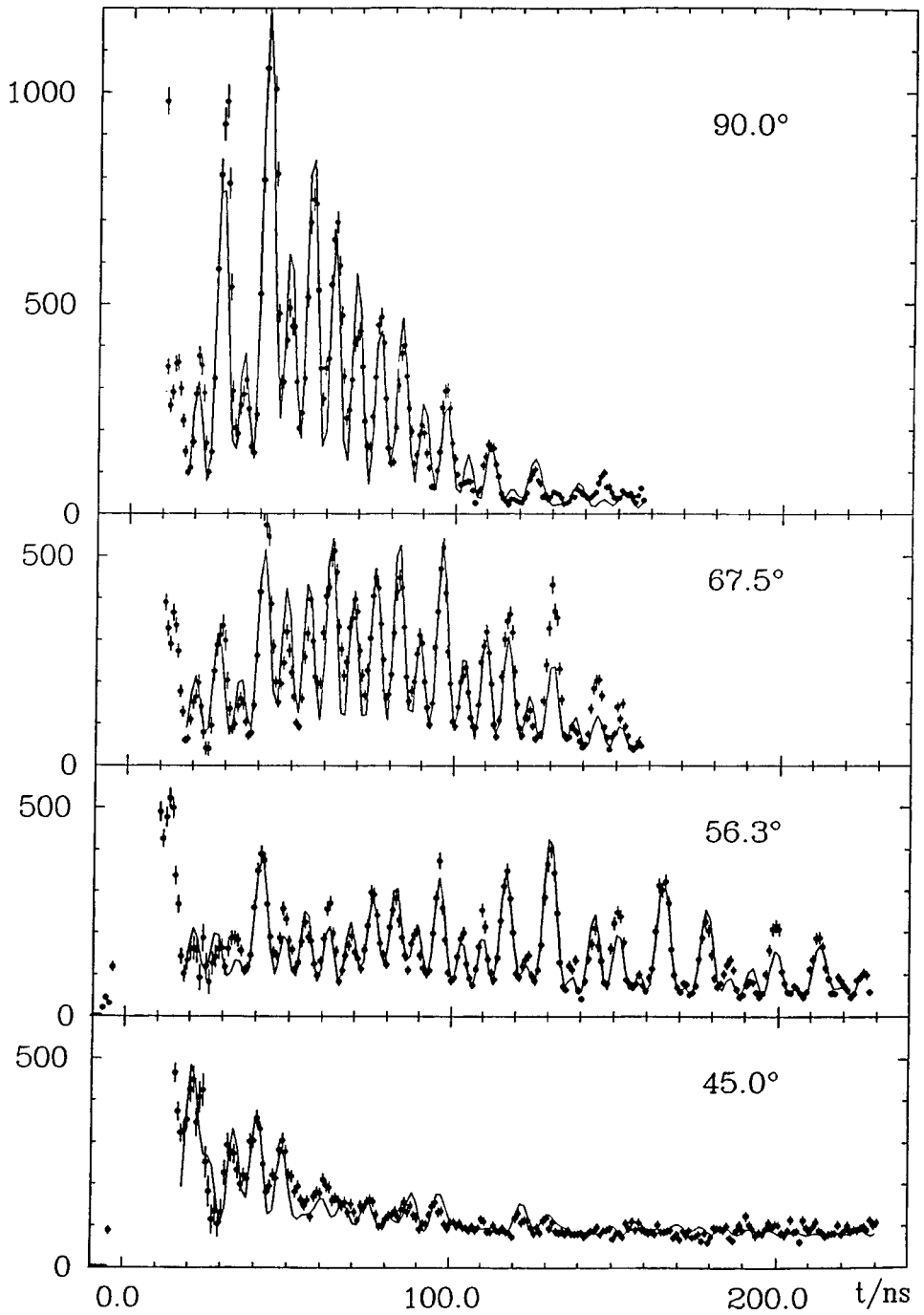

Figure 2. Time spectra of the d-sites in YIG for the (0 0 2) pure nuclear reflection. Only the d_1- and d_2-sites contribute to the reflection. The angle between the crystal axis [1 0 0] and the applied external field $\mathbf{B}_{ext}$ was varied (from [27]).

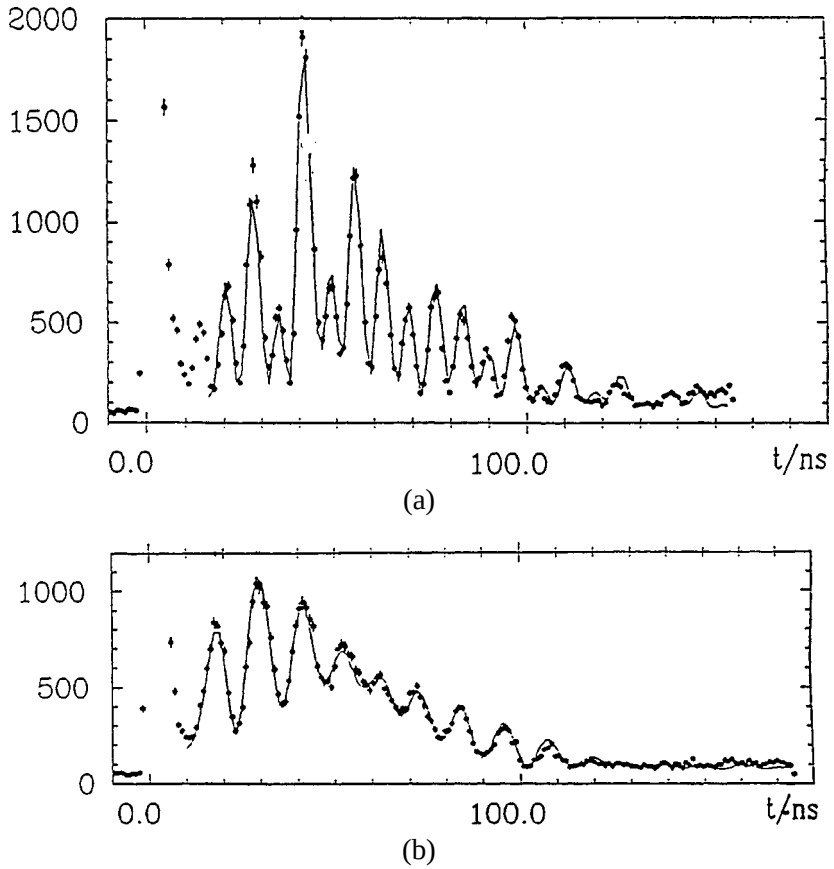

Figure 3. Time spectra of the d-sites in YIG for the (0 0 2) (a,b) and (0 0 10) (c) pure nuclear reflections. The alignment of the internal magnetic field $\mathbf{B}_{\rm hf}$ with respect to the incoming $\mathbf{k}_{\rm in}$ and the polarization $\hat{\varepsilon}_{\rm in}$ changes the time response. (a) $\mathbf{B}_{\rm hf} \perp \mathbf{k}_{\rm in}$ and $\mathbf{B}_{\rm hf} \parallel \hat{\varepsilon}_{\rm in}$ (from [26]), (b) $\mathbf{B}_{\rm hf} \parallel \mathbf{k}_{\rm in}$ and $\mathbf{B}_{\rm hf} \perp \hat{\varepsilon}_{\rm in}$ (from [26]), (c) $\mathbf{B}_{\rm hf} \perp \mathbf{k}_{\rm in}$ and $\mathbf{B}_{\rm hf} \perp \hat{\varepsilon}_{\rm in} \perp \mathbf{k}_{\rm in}$ (from [29]).

At first glance these spectra may look complicated. But exploiting the polarization dependence of the scattering and the 100% linear polarization of synchrotron radiation one may simplify the spectra. This is shown in figure 3 for the (0 0 2) and (0 0 10) reflections in YIG and for different orientations of $\mathbf{B}_{\rm hf}$, $\mathbf{k}_{\rm in}$, and $\hat{\varepsilon}_{\rm in}$.

Ignoring in the following the small perturbation caused by the electric interaction and using the (0 0 2) reflection with the small Bragg angle of 4° we get the following eigenpolarizations and excite the following nuclear transitions: (a) linear (σ), $\Delta m = \pm 1$; (b) left-circular with $\Delta m = +1$, right-circular with $\Delta m = -1$; (c) linear (π) with $\Delta m = 0$.

Case (a) is described by eq. (3.2). One may nicely recognize the high–low modulation of the intensity of adjacent maxima due to the interference term $\cos((1/2)\Omega_{\rm M}(1,6)\cdot t)\cos((1/2)\Omega_{\rm M}(3,4)\cdot t)$. Case (b) corresponds to eq. (3.3) and gives a simple pattern with one frequency. However, the contrast is reduced due to

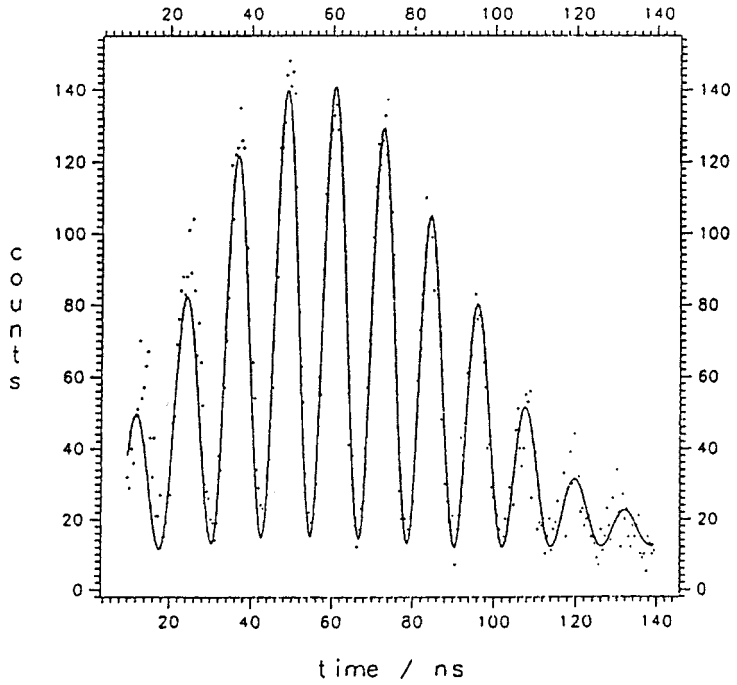

(c)

Figure 3. (Continued.)

the unequal oscillator strengths. In the last case, as seen in the figure, we get only one beat frequency for the magnetic interaction from the two $\Delta m = 0$ transitions. This corresponds to the case described by eq. (3.1). The high contrast of the beat pattern caused by the two transitions of equal strength is nicely seen.

The beat pattern caused by the electric interaction stays for all cases and gives the slow overall modulation. Without losing information on the hyperfine parameters the spectrum in figure 3(c) is very much simplified, making the data evaluation easier.

5.4. Direction of hyperfine fields

The effective magnetic field at the position of a nucleus is the vector sum of the internal hyperfine field $\mathbf{B}_{\mathrm{hf}}$ and an external field $\mathbf{B}_{\mathrm{ext}}$ of any origin:

$$\mathbf{B}_{\mathrm{eff}} = \mathbf{B}_{\mathrm{hf}} + \mathbf{B}_{\mathrm{ext}}.$$

Let us disregard for the moment complications which might effect the deviation of $\mathbf{B}_{\mathrm{ext}}$ from the applied field, e.g., demagnetization factors or the Knight shift [30], and assume that it is possible to fully magnetize a sample. Then the above given

vector equation reduces to either of the two scalar equations combining only absolute values:

$$B_{\text{eff}} = B_{\text{hf}} + B_{\text{ext}} \quad \text{or} \quad B_{\text{eff}} = B_{\text{hf}} - B_{\text{ext}},$$

where normally $B_{\text{hf}} \gg B_{\text{ext}}$ and an additional sign attributed to B_{hf} is defined by the convention:

- "positive hyperfine field" means: $\mathbf{B}_{\text{hf}} \uparrow\uparrow \mathbf{B}_{\text{ext}}$,
- "negative hyperfine field" means: $\mathbf{B}_{\text{hf}} \downarrow\uparrow \mathbf{B}_{\text{ext}}$.

The magnetic dipole interaction with a nuclear magnetic moment $\boldsymbol{\mu}_n$ introduces an energy shift ΔE_{M} depending on B_{ext}:

$$\Delta E_{\text{M}}(B_{\text{ext}}) = -\boldsymbol{\mu}_n \cdot \mathbf{B}_{\text{eff}}(B_{\text{ext}}),$$

which, if its variation with B_{ext} is detectable, allows one to deduce the value and the sign of the hyperfine field, i.e., its direction with respect to $\mathbf{B}_{\text{ext}}$.

This technique does not work in experiments where due to $B_{\text{ext}} \ll B_{\text{hf}}$ a sufficient variation of the energy shift can not be observed or even vanishes, if $B_{\text{ext}} \simeq 0$. This situation is often encountered in easily magnetized samples considered here where diffraction from single crystals with easy magnetization planes or axes is employed. On the other hand, diffraction at a Bragg angle $\Theta_{\text{B}} \neq 0°, 90°$ offers the advantage of a uniquely defined scattering plane $(\mathbf{k}_{\text{in}}, \mathbf{k}_{\text{out}})$ in contrast to the rotational symmetry in nuclear forward scattering or in conventional Mössbauer transmission experiments. Therefore, the experimental situation here is comparable to, e.g., $\gamma\gamma$-perturbed angular correlation experiments where at angles $\Theta = \angle(\gamma_1, \gamma_2) \neq 0°, 180°$ the plane $(\mathbf{k}_1, \mathbf{k}_2)$ serves as a reference. In the preferred geometry where $\mathbf{B}_{\text{ext}}$ is chosen perpendicular to this plane, the determination of the sign of B_{hf} is well known, e.g., the time-differential $\gamma_1\gamma_2$-coincidence rate contains an angular phase factor $\pm\omega_{\text{L}}t$, the sign of which is measured and uniquely determines the sign of the hyperfine field, if the applied field and the magnetic moment of the nucleus are known [31].

The effect of phase factors was already mentioned in early nuclear diffraction experiments of the Hamburg group [27,32] where even then quantum beats in the time spectra of scattered synchrotron radiation by YIG single crystals were observed, when the contributing scatterers on two different sites oscillate at exactly the same nuclear frequency. But it is the different phase factor of the two eigenfunctions describing the emission into the Bragg angle Θ_{B}, which leads to a beating, and is only reproduced correctly by application of the full dynamical theory of nuclear diffraction, where the Born approximation predicts zero scattering intensity. The phase difference in the experiments due to the small Bragg angle of $\simeq 4°$ for the (0 0 2) reflection in YIG is relatively small.

Another indication of the importance of the phase factor, which has a definite sign and bears, therefore, the information on the direction of $\mathbf{B}_{\text{hf}}$, was seen in further diffraction experiments on YIG [33] when the direction of $\mathbf{B}_{\text{hf}}$ was deliberately reversed. The time spectra for both settings differed markedly and could only be fitted

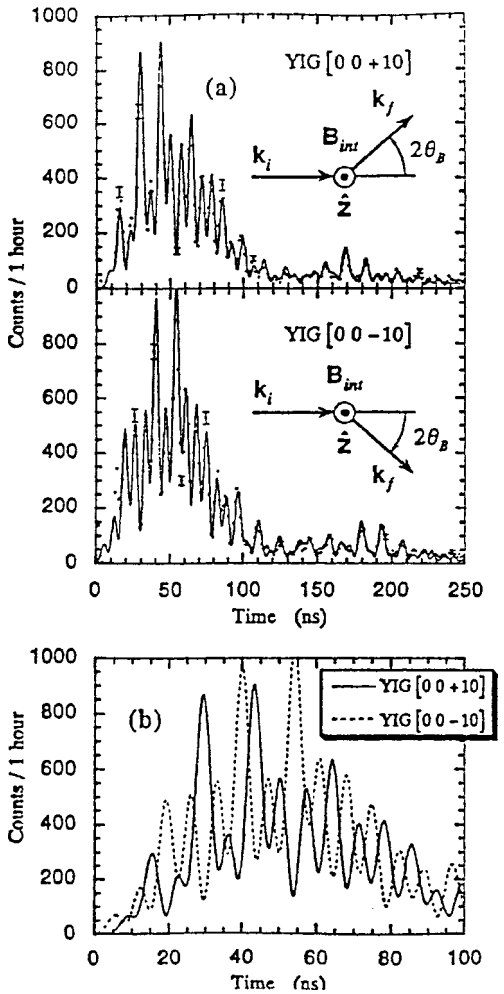

Figure 4. (a) Time spectra for the (0 0 +10) and (0 0 −10) reflections of YIG; (b) expanded, superimposed view of the fits to the data of (a) (from [34]).

if a magnetic field reversal was implemented in the program package (CONUSS [14]) but no definite conclusion on the real direction of $\mathbf{B}_{\mathrm{hf}}$ was drawn.

Eventually it was the Stanford group that devoted full attention to this effect in an experiment at the Cornell High Energy Synchrotron Source (CHESS) [34]. By choosing the (0 0 +10) reflection in YIG with the much larger Bragg angle of $\simeq 20^\circ$ they could fully clarify the situation and trace back the observed quantum beat shift to a purely geometrical angular shift of $\Delta\varphi_m = m \cdot 2\Theta_{\mathrm{B}}$ in each of the two most prominently interfering photon states ($m = +1$ and $m = -1$), i.e., lines one and six, respectively. The intensity function describing the beating of these two lines is given by

$$I_+(t) \propto 1 + \cos\bigl(\Omega_{\mathrm{M}}(1,6) \cdot t - 4\Theta_{\mathrm{B}}\bigr).$$

Using the (0 0 −10) reflection would result in

$$I_{-}(t) \propto 1 + \cos\bigl(\Omega_{\mathrm{M}}(1,6)\cdot t + 4\Theta_{\mathrm{B}}\bigr),$$

so the total angular shift between these two settings would effectively be $8\Theta_{\mathrm{B}}$.

Instead of changing the crystal's and the detector's position into the mirrored Bragg reflection (0 0 −10) setting, the authors took advantage of the fact that the simple reversal of the external field, i.e., the simultaneous inversion of the hyperfine field, has the identical result as changing signs of the angular phase factors. Then the total phase difference between the two settings with reversed field directions is $8\Theta_{\mathrm{B}}$, which in this experiment gives the almost maximum shift of $\simeq 160^{\circ}$ (see figure 4).

While this is a beautiful demonstration of how a purely geometrical effect shows up as a phase shift which can be clearly observed in an interference measurement, it also offers access to an unambiguous determination of the sign of the magnetic hyperfine field. The sign of the measured phase difference $+8\Theta_{\mathrm{B}}$ or $-8\Theta_{\mathrm{B}}$ immediately tells the direction of the hyperfine field. This is based on the noncollinear direction of the photon vectors $\mathbf{k}_{\mathrm{in}}$ and $\mathbf{k}_{\mathrm{out}}$ similar to $\gamma\gamma$-perturbed angular correlation experiments in external fields, where γ_1, γ_2 coincidences are recorded for noncollinear emission directions of the two photons.

Eventually, from the measured direction of the hyperfine field and knowing the direction of the external applied field, a fact which very often in normal laboratory work is likely to be overlooked, especially in arrangements with permanent magnets, the sign of B_{hf} is deducible. Following this procedure the Stanford experiment gave a direct proof of the known result, that the ^{57}Fe nuclei on the d-sites in YIG, i.e., the positions with local tetrahedral symmetry that build up the beat pattern for the (0 0 ±10) reflections, experience a negative magnetic hyperfine field.

6. Antiferromagnetic systems

$FeBO_3$ and α-Fe_2O_3 are representatives for (canted) antiferromagnetic systems crystallizing in a rhombohedral calcite structure, D^6_{3d} [35–37]. They each have two molecules per unit cell which lead to the formation of magnetic sublattices below the Néel temperature (348 K for $FeBO_3$ and 948 K for α-Fe_2O_3). The magnetic moments lie in the (1 1 1)-plane with two adjacent planes being antiferromagnetically coupled. Because the antiferromagnetic moments are canted, there is a small ferromagnetic moment within the (1 1 1)-plane. A small external field is sufficient to orient the antiferromagnetic moments.

In these systems the sublattices giving rise to pure nuclear reflections are determined by the antiferromagnetic sublattice structure. Since the magnetic moments lie in (nearly) antiparallel directions for adjacent planes, the polarization for each transition for these planes is different, i.e., the lattice spacing is doubled and a pure nuclear

reflection is built up. In the rhombohedral representation the following reflections are pure nuclear reflections:

$$h = k = l = 2n + 1 \quad \text{with } n \in \mathbb{Z}.$$

In the following we will discuss for $FeBO_3$ general aspects of hyperfine spectroscopy and will show in the case of α-Fe_2O_3 how hyperfine spectroscopy may benefit from an additional polarization analysis of the diffracted beam.

As a third example we will briefly discuss the orthorhombic ironborate Fe_3BO_6, which is a weak ferromagnet of structure D_{2h}^{16} below the Néel temperature at about 508 K. The easy axis of this ferrimagnet changes its orientation from [1 0 0] to [0 0 1] at a spin reorientation temperature of about 408 K.

6.1. *$FeBO_3$*

$^{57}FeBO_3$ crystals can be grown as nearly perfect single crystals from the melt [39]. They have a green colour. In the investigations platelets with sizes of about 100 mm^2 and thicknesses of 50–150 μm with (1 1 1)-surface have been used.

Figure 5 shows a typical time spectrum for $FeBO_3$ with $\mathbf{k}_{\text{in}} \perp \mathbf{B}_{\text{hf}}$ and $\mathbf{B}_{\text{hf}} \parallel \hat{\varepsilon}_{\text{in}}$. Again nearly all features of this quantum beat spectrum can be understood in the Born approximation. The case corresponds to eq. (3.2). Using the correct spatial phase the cosine dependence becomes a sine dependence, expressing the character of a pure nuclear reflection.

$$I(t) \propto \mathrm{e}^{-\Gamma t/\hbar} \left| \sin\left(\frac{1}{2}\Omega_{\text{M}}(1,6)\cdot t\right) - \frac{1}{3}\mathrm{e}^{-\mathrm{i}\Delta\Omega\cdot t} \sin\left(\frac{1}{2}\Omega_{\text{M}}(3,4)\cdot t\right)\right|^2. \tag{6.1}$$

The factor $\mathrm{e}^{-\mathrm{i}\Delta\Omega\cdot t}$ with $\hbar\Delta\Omega = (1/2)eQV_{zz}$ takes into account the shift between the center of the $(3,4)$-lines and the center of the $(1,6)$-lines which is due to the

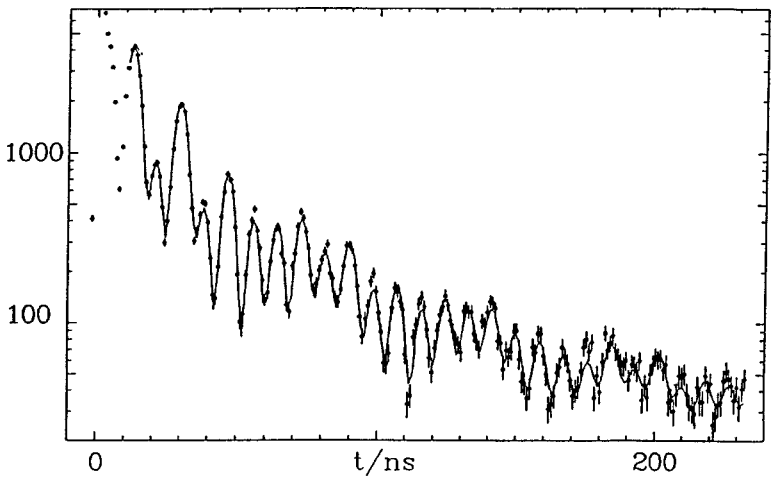

Figure 5. Time spectrum of the (1 1 1) pure nuclear reflection of $FeBO_3$.

small electric interaction. The pattern is dominated by the high frequency $\Omega_{\mathrm{M}}(1,6)$ which arises from the interference between the strong lines one and six. The very perceptible modulation of a "high–low" pattern is caused by the interference term $\sin((1/2)\Omega_{\mathrm{M}}(1,6)\cdot t)\cdot\sin((1/2)\Omega_{\mathrm{M}}(3,4)\cdot t)$ [40].

6.1.1. Reissverschluss effect

Another interesting feature is the asymmetry in the quantum beat amplitudes above and below the Bragg angle [40]. This asymmetry gives a direct measure of the weak quadrupole interaction. In the absence of a quadrupole interaction, the reflectivity has an inversion symmetry with respect to the deviation $\delta\Theta$, i.e. $|R(t,\delta\Theta)|^2 = |R(t,-\delta\Theta)|^2$. The quadrupole interaction removes the inversion symmetry, leading to an asymmetry in the time response

$$\left|R(t,\delta\Theta)\right|^2-\left|R(t,-\delta\Theta)\right|^2 \propto -\sin(\Delta\Omega\cdot t)\cdot\left[\sin\left(\frac{1}{2}\Omega_{\mathrm{M}}(1,6)\cdot t\right)\cdot\sin\left(\frac{1}{2}\Omega_{\mathrm{M}}(3,4)\cdot t\right)\right], \tag{6.2}$$

which directly gives $\Delta\Omega$, including the sign. Because of the proportionality to $\sin((1/2)\Omega_{\mathrm{M}}(1,6)\cdot t)$ this appears as a "Reissverschluss" (zipper) asymmetry in the amplitudes of the fast quantum beats above and below the Bragg angle.

6.1.2. Temperature dependence

The measurement of the temperature dependence of the hyperfine splitting is reported in [41]. Time spectra of the (3 3 3) pure nuclear reflection were measured in the temperature range between room temperature and the Néel temperature. They show a strong quantum beat dilation due to magnetization breakdown. The evaluation with the dynamical theory allowed the determination of the magnetic fields with an error

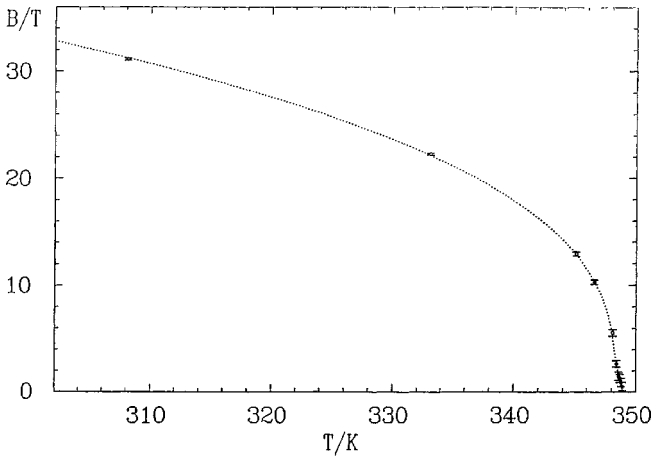

Figure 6. Temperature dependence of the internal field $\mathbf{B}_{\mathrm{hf}}$ in $FeBO_3$ obtained from the fit of the corresponding time spectra [33,41].

less than 0.2 T (figure 6). As the pure nuclear reflection is built up due to the antiferromagnetic coupling, the pure nuclear reflection vanishes at the Néel temperature.

6.2. α-Fe_2O_3 – Polarization analysis

α-Fe_2O_3 shows the same behaviour as $FeBO_3$ with respect to the hyperfine interaction. Therefore, the previous discussion on $FeBO_3$ also holds for α-Fe_2O_3. First investigations on this system have been carried out by the Brookhaven group [42–44] followed by the Japanese group [22].

In [45] the authors show that one may analyze the polarization of the diffracted beam and that the theoretical predictions fit the experimental results. Applying this method to hyperfine spectroscopy one may gain more information on the system under investigation. In the following scenario the time spectra would look the same, only the polarization of the diffracted beam is different. For shallow angles an antiferromagnetic system will rotate the σ-polarization of the synchrotron radiation beam to the π-polarization states when the magnetic moments are aligned parallel to the $\mathbf{k}_{in}$-vector. In the case of ferromagnetic coupling, however, the σ-polarization would stay. In both

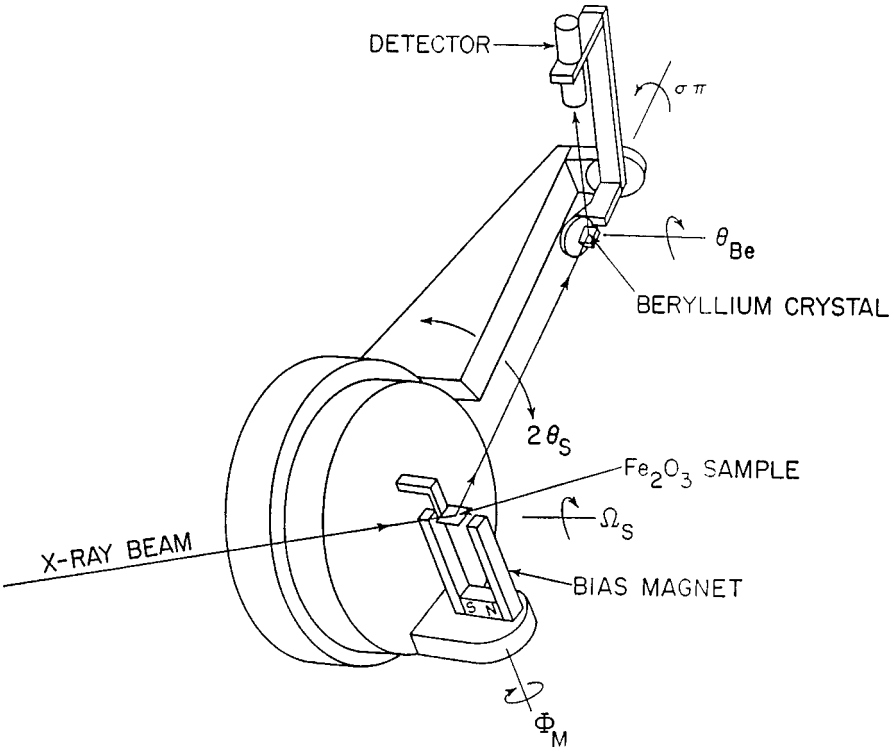

Figure 7. Set-up of the diffractometer which carries the sample and its polarizing magnet. The magnetic field direction can be rotated about the sample diffraction vector. Polarization analysis of the diffracted beam is done by the beryllium crystal and its detector. The scattering plane of the beryllium can be rotated around the diffracted beam from the sample (from [45]).

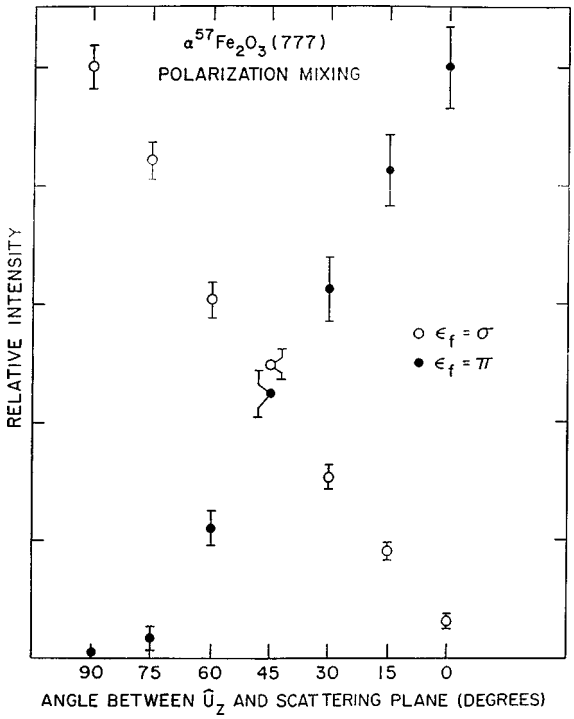

Figure 8. Intensity scattered into the σ- and π-polarization directions as a function of the orientation of the magnetic quantization axis (from [45]).

cases an external alignment field is assumed perpendicular to $\mathbf{k}_{in}$ and parallel to the incomimg σ-polarization, i.e., the experimental set-up is the same. The method of polarization analysis allows one to distinguish between the two cases.

The instrument needs an additional polarization analyzer stage which has been installed on the main 2Θ-arm of the diffractometer (figure 7). This analyzer stage consists of another Θ–2Θ stage carrying the analyzer crystal and the detector system. In the original set-up [45] a Be crystal with a small mosaic spread was used in order to match the divergence of the synchrotron radiation beam from a wiggler station. As analyzer a crystal with a Bragg angle of 45° at the desired energy has to be chosen. This is the Brewster angle for X-rays where only one polarization state is diffracted. Figure 8 shows nicely the dependence of the diffracted intensity in the σ- and π-channel, respectively, with respect to the quantization axis of the α-Fe_2O_3 crystal, i.e., the axis of the magnetic moments of the Fe atoms.

6.3. Fe_3BO_6

Iron orthoborate Fe_3BO_6 grows as thin crystal platelets of a brownish colour. Their crystallographic and magnetic structure was extensively studied [38,39,46–48] with different techniques. We will here concentrate on the resonant nuclear diffraction

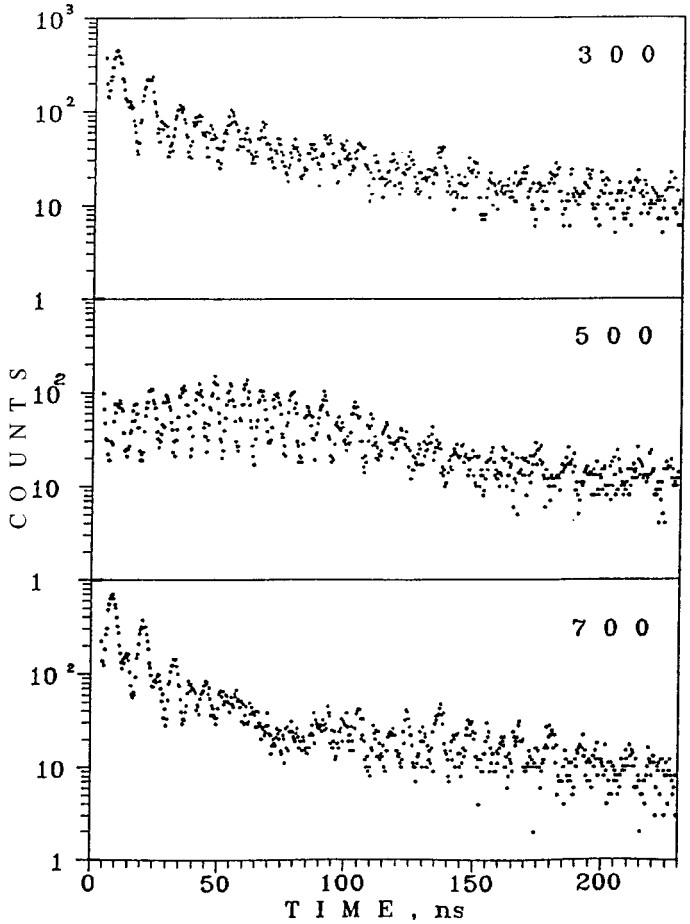

Figure 9. Time spectra of the pure nuclear reflections (3 0 0), (5 0 0) and (7 0 0) of $^{57}Fe_3BO_6$ (from [50]).

experiments using almost perfect single crystals of $^{57}Fe_3BO_6$ in Laue and Bragg geometry. The magnetic structure below the Néel point at about 508 K is made up of two antiferromagnetic sublattices – one built by the eight iron atoms in the 8d positions, the other by the four iron atoms in the 4c positions. Both lattices have their spontaneous antiferromagnetic axis aligned with the [1 0 0]-axis above the spin reorientation temperature at about 408 K, while below this temperature both spin systems are aligned with the [0 0 1] axis. At least one sublattice does not form a perfect antiferromagnet, i.e., a canting angle exists, which leads to a small ferromagnetic moment, which points below 408 K into the [1 0 0] direction, and above it into the [0 0 1] direction. Recent results from measurements with a polarized Mössbauer source, combined with NFS studies, indicate that all data can be fitted consistently if for the 4c positions a canting angle of about 10° is assumed [49].

Time spectra of different Bragg reflections were recorded in an experiment at DORIS (DESY, Hamburg) to reveal the interference of scattering from the different

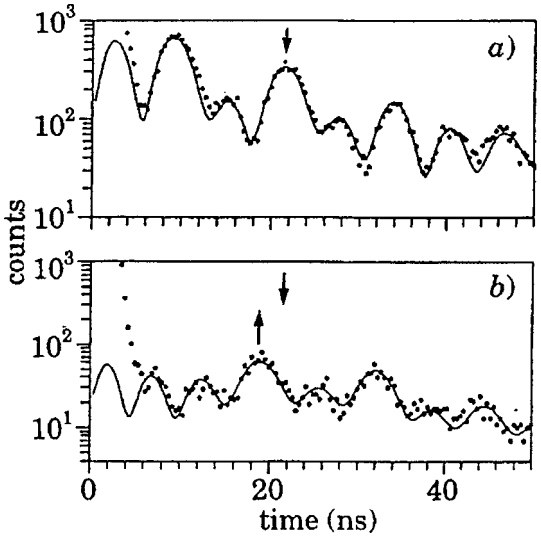

Figure 10. Time spectra for the (7 0 0) Bragg reflection (a) and the (0 0 3) Laue reflection from a 43 μm thick $^{57}Fe_3BO_6$ crystal (b). The solid lines are fits based on the dynamical theory for nuclear resonant scattering (from [51]).

positions of the nuclei in non-equivalent sublattices [50]. Figure 9 shows the result for the pure nuclear reflections (3 0 0), (5 0 0), and (7 0 0). The time spectrum of the (3 0 0) reflection resembles the quantum beat pattern of a simple antiferromagnet (compare $^{57}FeBO_3$), which is in agreement with the fact that in this case only the 8d sublattice contributes to the scattering. The time spectra of the (5 0 0) and (7 0 0) reflections show a slow modulation, which revealed that in these cases interference with the scattering from the 4c sublattice, where the hyperfine field and consequently the oscillator frequencies are shifted with respect to the 8d sublattice, is observed, either destructive in the (5 0 0), or constructive in the (7 0 0) reflection. Closer inspection of the spectra gives evidence that also the fast quantum beats for (5 0 0) and (7 0 0) are in antiphase, which is in complete agreement with the expectations of the dynamical theory for nuclear resonant scattering [12].

Another feature of nuclear diffraction from the Fe_3BO_6 crystals was nicely demonstrated when the time spectrum of the (7 0 0) Bragg reflection was compared with the (0 0 3) Laue reflection. In both cases the scattering from the two antiferromagnetic sublattice positions interferes constructively [51]. Figure 10 shows the results for the (7 0 0) Bragg case and the (0 0 3) Laue case for a platelet of 43 μm thickness. One of the pronounced effects in the Laue spectrum is the shift of comparable beat maxima to earlier times with increasing thickness. Again, this is in total agreement with the dynamical theory (see solid lines indicating the fits based on the theory); in the Laue case, the interfering hyperfine components have different phase velocities due to the complicated dispersion law, and therefore their relative phases at the exit surface of the crystal are thickness dependent.

7. Conclusion

These investigations on single crystals were certainly triggered by the need to suppress the overwhelming background by Coulomb scattering from the nuclear scattered signal. Nevertheless, Nuclear Bragg Diffraction (NBD) became a field of research in its own right with its special merits. We have discussed some of these, such as the "Reissverschluss" effect, the determination of the direction of the magnetic hyperfine field and the polarization analysis. In the case of Fe_3BO_6 a better understanding of the magnetic structure could be gained in a rather straightforward way. For a while the new techniques such as NFS and Nuclear Inelastic Scattering (NIS) have attracted much attention. However, recently, the diffraction studies got a new impetus.

In the diffusion work (see section IV.2.6 of this issue) it became advantageous to work in Bragg geometry instead of NFS geometry. In NFS studies one works in transmission geometry, where very thin single crystals are required. This problem is avoided in Bragg geometry where crystals as grown might be used, allowing one to investigate, e.g., very brittle material. First experiments on diffusion have been carried out on Fe_3Si [52] in Bragg geometry.

Another example is the structure determination. In the case of quasi-crystals such as $Al_{62}Cu_{25.5}Fe_{12.5}$ there exists a controversial discussion on their structure. Especially the sites which are occupied by iron ions seem questionable. In this case NBD should be able to contribute to this debate. First experiments, by measuring over 40 independent nuclear as well as electronic reflections, have been carried out [53]. The result of the data evaluation should clearly distinguish between different theoretical models.

Furthermore, these two examples, using mosaic crystals, show that with the new high intense synchrotron radiation sources there is no longer a need for highly perfect single crystals as in the early days. As grown crystals can be investigated, which should pave the way for further applications.

References

[1] G.V. Smirnov, Hyp. Interact. 27 (1986) 203;
U. van Bürck, Hyp. Interact. 27 (1986) 219.
[2] E. Gerdau, R. Rüffer, H. Winkler, W. Tolksdorf, C.P. Klages and J.P. Hannon, Phys. Rev. Lett. 54 (1985) 835.
[3] E. Gerdau, R. Rüffer, R. Hollatz and J.P. Hannon, Phys. Rev. Lett. 57 (1986) 1141.
[4] R. Rüffer, E. Gerdau, R. Hollatz and J.P. Hannon, Phys. Rev. Lett. 58 (1987) 2359.
[5] R. Hollatz, R. Rüffer and E. Gerdau, Hyp. Interact. 42 (1988) 1141.
[6] `http://www.esrf.fr/exp_facilities/ID18/handbook/handbook.html`.
[7] J.P. Hannon and G.T. Trammell, Phys. Rev. 186 (1969) 306.
[8] G.T. Trammell and J.P. Hannon, Phys. Rev. B 18 (1978) 165; Phys. Rev. B 19 (1979) 3835.
[9] J.P. Hannon and G.T. Trammell, Physica B 159 (1989) 161.
[10] A.M. Afanas'ev and Yu. Kagan, Zh. Eksper. Teoret. Fiz. Pis. Red. 2 (1965) 130 (JETP Lett. 2 (1965) 81).
[11] Yu. Kagan, A.M. Afanas'ev and V.G. Kohn, Phys. Lett. A 68 (1978) 339.
[12] Yu. Kagan, A.M. Afanas'ev and V.G. Kohn, J. Phys. C 12 (1979) 615.

[13] B.W. Batterman and H. Cole, Rev. Mod. Phys. 36 (1964) 681.
[14] W. Sturhahn and E. Gerdau, Phys. Rev. B 49 (1994) 9285.
[15] R.Rüffer, Ph.D. thesis, Universität Hamburg, Hamburg (1985), Interner Bericht, HASYLAB 86-02 (April 1986).
[16] R. Rüffer, R. Hollatz, E. Gerdau, U. van Bürck and J.P. Hannon, Hyp. Interact. 42 (1988) 1161.
[17] R. Rüffer and A.I. Chumakov, Hyp. Interact. 97/98 (1996) 589.
[18] E.E. Alp, T.M. Mooney, T. Toellner and W. Sturhahn, Hyp. Interact. 90 (1994) 323.
[19] SPring-8 Annual Reports (1996, 1997 and 1998).
[20] R. Rüffer, D. Giesenberg, H.D. Rüter, R. Hollatz, E. Gerdau, J. Metge, K. Ruth, W. Sturhahn, M. Grote and R. Röhlsberger, Hyp. Interact. 58 (1990) 2467.
[21] ESRF: `http://www.esrf.fr/exp_facilities/ID18/handbook/handbook.html;` APS: `http://www.aps.anl.gov/sricat/3id.html;` SPring-8: `http://www.spring8.or.jp/ENGLISH/facility/bl/PublicBeamline/BL09XU/index.html.`
[22] S. Kikuta, in: *Nuclear Resonant Scattering Using Synchrotron Radiation from an X-ray Undulator in Resonant Anomalous X-ray Scattering, Theory and Applications*, eds. G. Materlik, C.J. Sparks and K. Fischer (Elsevier Science, Amsterdam, 1994) p. 635.
[23] G. Winkler, *Magnetic Garnets*, Vieweg Tracts in Pure and Applied Physics, Vol. 5 (Vieweg, Braunschweig/Wiesbaden, 1981).
[24] H. Winkler, R. Eisberg, E. Alp, R. Rüffer, E. Gerdau, S. Lauer, A.X. Trautwein, M. Grodzicki and A. Vera, Z. Phys. B 49 (1983) 331.
[25] R. Rüffer, J. Metge, H.D. Rüter, W. Sturhahn and E. Gerdau, Hyp. Interact. 71 (1992) 1353.
[26] H.D. Rüter, R. Rüffer, R. Hollatz, W. Sturhahn and E. Gerdau, Hyp. Interact. 58 (1990) 2477.
[27] R. Rüffer, E. Gerdau, H.D. Rüter, W. Sturhahn, R. Hollatz and A. Schneider, Phys. Rev. Lett. 63 (1989) 2677.
[28] W. Sturhahn, E. Gerdau, R. Hollatz, R. Rüffer, H.D. Rüter and W. Tolksdorff, Europhys. Lett. 14 (1991) 821.
[29] ESRF Annual Report (1993) p. 87.
[30] G.C. Carter, L.H. Bennett and D.J. Kahan, Metallic Shifts in NMR, Progr. Math. Sci. 20 (1977).
[31] H. Frauenfelder and R.M. Steffen, in: *Alpha-, Beta- and Gamma-Ray Spectroscopy*, Vol. 2, ed. K. Siegbahn (North-Holland, Amsterdam, 1968) p. 1156.
[32] R. Hollatz, W. Sturhahn, H.D. Rüter and E. Gerdau, Hyp. Interact. 58 (1990) 2457.
[33] R. Hollatz, Ph.D. thesis, Universität Hamburg, Hamburg (1992).
[34] D.E. Brown, J. Arthur, A.Q.R. Baron, G.S. Brown and S. Shastri, Phys. Rev. Lett. 69 (1992) 699; D.E. Brown, Ph.D. thesis, SSRL at SLAC, Stanford University, Stanford (1993).
[35] I. Bernal, C.W. Struck and J.G. White, Acta Cryst. 16 (1963) 849.
[36] R. Diehl, Solid State Comm. 17 (1975) 743.
[37] B.T.M. Willis and H.P. Rooksby, Proc. Phys. Soc. [London] B 65 (1952) 950.
[38] R. Diehl and G. Brandt, Acta Cryst. B 31 (1975) 1662.
[39] M. Kotrbova, S. Kadeckova, J. Novak, J. Bradler, G.V. Smirnov and Yu.V. Shvyd'ko, J. Crystal Growth 71 (1985) 607.
[40] U. van Bürck, R.L. Mössbauer, E. Gerdau, R. Rüffer, R. Hollatz, G.V. Smirnov and J.P. Hannon, Phys. Rev. Lett. 59 (1987) 355.
[41] H.D. Rüter, R. Rüffer, E. Gerdau, R. Hollatz, A.I. Chumakov, M.V. Zelepukhin, G.V. Smirnov and U. van Bürck, Hyp. Interact. 58 (1990) 2473.
[42] G. Faigel, D.P. Siddons, J.B. Hastings, P.E. Haustein and J.R. Grover, Phys. Rev. Lett. 58 (1987) 2699
[43] G. Faigel, D.P. Siddons, J.B. Hastings, P.E. Haustein, J.R. Grover and L.E. Berman, Phys. Rev. Lett. 61 (1988) 2794

[44] J.B. Hastings, D.P. Siddons, G. Faigel, L.E. Berman, P.E. Haustein and J.R. Grover, Phys. Rev. Lett. 63 (1989) 2252.
[45] D.P. Siddons, J.B. Hastings, G. Faigel, L.E. Berman, P.E. Haustein and J.R. Grover, Phys. Rev. Lett. 62 (1989) 1384.
[46] B. Andlauer and R. Diehl, Physica B 89 (1977) 50.
[47] R. Wolfe, R.D. Pierce, M. Eibschütz and J.W. Nielsen, Solid State Commun. 7 (1969) 949.
[48] A.S. Kamzin and L.A. Grigor'ev, Zh. Eksper. Teoret. Fiz. 104 (1993) 3489 (Sov. Phys. JETP 77 (1993) 658).
[49] J. Jäschke, Ph.D. thesis, Universität Hamburg, Hamburg (1999);
J. Jäschke, H.D. Rüter, E. Gerdau, G.V. Smirnov, W. Sturhahn and J. Pollmann, Nucl. Instrum. Methods B 155 (1999) 189.
[50] A.I. Chumakov, G.V. Smirnov, M.V. Zelepukhin, U. van Bürck, E. Gerdau, R. Rüffer and H.D. Rüter, Hyp. Interact. 71 (1992) 1341.
[51] A.I. Chumakov, G.V. Smirnov, M.V. Zelepukhin, U. van Bürck, E. Gerdau, R. Rüffer and H.D. Rüter, Europhys. Lett. 17 (1991) 269.
[52] H. Thieß, B. Sepiol, G. Vogl and R. Rüffer, to be published (1999).
[53] M. Capitan, R. Brand, G. Coddens and R. Rüffer, to be published (1999).